Design and Characterization of Electroresponsive Polymers Based on the Johnsen-Rahbek Effect

by

Colin Dustin Ladd

B.A. Illinois College, 2013

Submitted to the Graduate Faculty of the

Kenneth P. Dietrich School of Arts and Sciences in partial fulfillment

of the requirements for the degree of

Master of Science

University of Pittsburgh

2015

UNIVERSITY OF PITTSBURGH

Dietrich School of Arts and Sciences

This thesis was presented

by

Colin Dustin Ladd

It was defended on

November 20, 2015

and approved by

Dr. Geoffrey Hutchison, Associate Professor, Department of Chemistry

Dr. Haitao Liu, Assistant Professor, Department of Chemistry

Thesis Director: Dr. Tara Meyer, Associate Professor, Department of Chemistry

Design and Characterization of Electroresponsive Polymers Based on the Johnsen-Rahbek Effect

Colin Dustin Ladd, M.S.

University of Pittsburgh, 2015

Electroactive polymers (EAPs) are synthetic materials that react to an electrical stimulus by altering one or more of their properties and have been of much interest in the fields of electrochemical actuation and electroadhesion. The majority of electroadhesive devices employing EAPs are governed by coulombic forces generated when an electric potential is applied across a dielectric polymer. Typically these devices are comprised of a stack of two composites, each consisting of a dielectric bound to an electrode, in which the dielectric layers are in contact. The coulombic force generated across the electroactive layers electrostatically adheres the composite together. However, there exists another electroadhesive force, the Johnsen-Rahbek (JR) force, which is expressed in the case of imperfectly insulating materials such as ion-containing polymers. Whereas coulombic electroadhesive systems have been studied extensively, materials that exhibit the JR force have received much less attention. Herein, the synthesis and characterization of structures composed poly(ethylene-*co*-acrylic acid) polymers with tetraalkylammonium counterions is described. A structure-activity relationship between the identity of the counterion and the thermal, electrical, mechanical, and electroresponsive attributes of the material is presented. The alkyl chain length of the quaternary ammonium counterions is found to influence the properties such that longer chain lengths result in both a lower initial modulus and a higher percentage change in modulus under an applied voltage.

TABLE OF CONTENTS

LIST OF TABLES

LIST OF FIGURES

LIST OF ABBREVIATIONS

AA	Acrylic acid
DSC	Differential scanning calorimetry
EAP	Electroactive polymer
EIS	Electrochemical impedance spectroscopy
JR	Johnsen-Rahbek
MPa	Megapascals
PEAA	Poly(ethylene-*co*-acrylic acid)
PEAA-TEAH	Poly(ethylene-*co*-tetraethylammonium acrylate)
PEAA-TMAH	Poly(ethylene-*co*-tetramethylammonium acrylate)
PEAA-TPAH	Poly(ethylene-*co*-tetrapropylammonium acrylate)
PIL	Poly ionic liquid
TEAH	Tetraethylammonium hydroxide
TGA	Thermogravimetric analysis
TMAH	Tetramethylammonium hydroxide
TPAH	Tetrapropylammonium hydroxide

1.0 INTRODUCTION

Stimuli-responsive polymer materials are synthetic structures that respond to chemical or physical changes to the system[1]. Included in this diverse array are materials that can be used as biocompatible materials for drug delivery[2] or tissue engineering[3], highly sensitive chemical sensors[4], and flexible actuators[5]. The stimuli employed include heat, such as in the case of some thermoplastic elastomers[6]; pH change, such as in pH-sensitive microparticles that change morphology in acidic microclimates[7]; and an electric potential in the case of polymers that undergo electrochemical changes such as oxidation or reduction.[8] The Meyer group is specifically interested in using electricity to stimulate changes in mechanical properties and has recently published work involving polymer hydrogels with these qualities.[9,10,11] In this work, the mechanical properties of metal ion-containing hydrogels were tuned by electrochemically oxidizing and reducing transition metal ions to strengthen (oxidized) or weaken (reduced) physical crosslinking of the polymer backbone.

To address some of the limitations experienced in the metal-ion containing hydrogel system, mainly that the electrochemical switching occurred slowly and required submerging in aqueous solution, a different mechanism for inducing electrically-controlled mechanical changes was pursued. Bar-Cohen and Zhang reviewed an array of electroactive polymer (EAP) actuators that undergo electromechanical changes via field-activated or ionic processes.[12] In these materials, an electric potential induces an accumulation of charge at a surface, which causes a deformation

of the structure which is used for physical actuation. The mechanism by which these EAP actuators generate force can also be applied to a layered system in order to induce an electroadhesive response. Generating, for instance, a positive charge at the surface of one layer could be interfaced with a layer with a negative charge. This electrostatic attraction would adhere the surfaces together and result in an overall stiffer structure due to the ability for a laminate to more efficiently transfer stresses through the whole of the structure.[13] The electrostatic mechanisms by which this electroadhesion can be achieved is reviewed in the following sections.

1.1 ELECTROADHESION

1.1.1 Coulombic adhesion

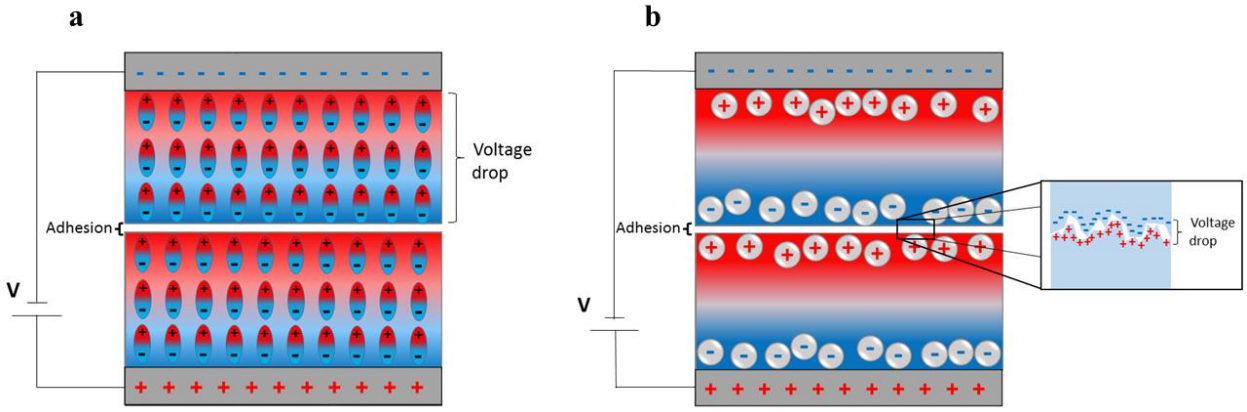

Figure 1. Comparison of a theoretical a) coulombic sandwich structure and b) Johnsen-Rahbek sandwich structure.

Previously, Bergamini et al. investigated the control of the stiffness of a composite structure wherein the mechanical properties are a function of the electrically-induced adhesion between

components or layers of field-activated polymers such as poly(vinylidene fluoride),[14,15] polyimide, and various other fluorinated polymers.[16] Due to the dielectric properties of these polymers, an applied electric field induces an alignment of dipoles that produces a coulombic force between the electrodes like that of a parallel plate capacitor (Figure 1a). The generated electrostatic force allows for a greater transfer of shear stresses throughout the sample which in turn stiffens the structure as a whole. Adhesive forces produced in this type of polymer system are governed by Coulomb's Law:

$$F = A\varepsilon_0(k_d V/D)^2/2 \qquad (1)$$

Where A is the electrode area, ε_0 is the permittivity of free space, k_d is the dielectric constant of the polymer, V is the applied voltage, and D is the thickness of the dielectric. Cantilever structures described by Bergamini et al. exhibit several-fold increases in flexural modulus upon applying a potential. However, the voltages required for these forces are in the thousands of volts (up to 5 kV reported) due to the practical constraints in the geometry of the structures. As the coulombic force is inversely proportional to the square of the thickness of the sample, a thinner dielectric results in a much greater force. There is, however, a limit to how thin a dielectric polymer layer can be fabricated without compromising the mechanical integrity of the material. Typically, a polymer layer incorporated into an electroadhesive structure must be at least 100-200 μm thick.[17] Due to this limitation, increasingly higher voltages are required to generate larger forces.

1.1.2 Johnsen-Rahbek adhesion

Larger adhesive forces at lower potentials can be accessed if the material contains mobile charged species. Polyelectrolytes of this type, which must have bulk resistivities below 10^4

MΩ·cm but can be as low as 10^{-4} MΩ·cm[18,19], allow a current to flow until capacitive charge is built up at the interface between layers as shown in Figures 1b and 2.[20] Due to the physical accumulation of a charge at the interface, the dielectric across which the electric field is applied is actually the nanoscale air gap between the surfaces. In this case, the force generated is defined by the Johnsen-Rahbek (JR) equation:

$$F = A_{eff}\,\varepsilon_0\,(k_g V_{eff}/g)^2/2 \qquad (2)$$

$$V_{eff} = [R_C/(R_C+R_V)]V \qquad (3)$$

Where A_{eff} is the effective area of contact; k_g is the dielectric constant of the gap (typically air, k_g = 1); g is the thickness of the air gap, dependent on surface roughness and pressure. The effective voltage at the interface (V_{eff}) is determined by the properties of the polyelectrolyte, where R_C is the contact resistance of the material; and R_V is the bulk resistivity.[21] In a system where the JR force is dominant, the air gap (typically on the scale of tens of nanometers) is orders of magnitude smaller than the thickness of the polyelectrolyte. As a result, much lower voltages are required to impart the same force as in a coulombic material. To optimize the JR force, the resistivity of the material can be tuned to improve the effective voltage by altering the identity of the mobile charge carriers. An ideal material for JR applications is as resistive as possible while still allowing for charge migration (resistivity < 10^4 MΩ·cm). These parameters still allow for an accumulation of electrostatic charge at the interface, while limiting the amount of energy lost to leakage current due to the material being too conductive.

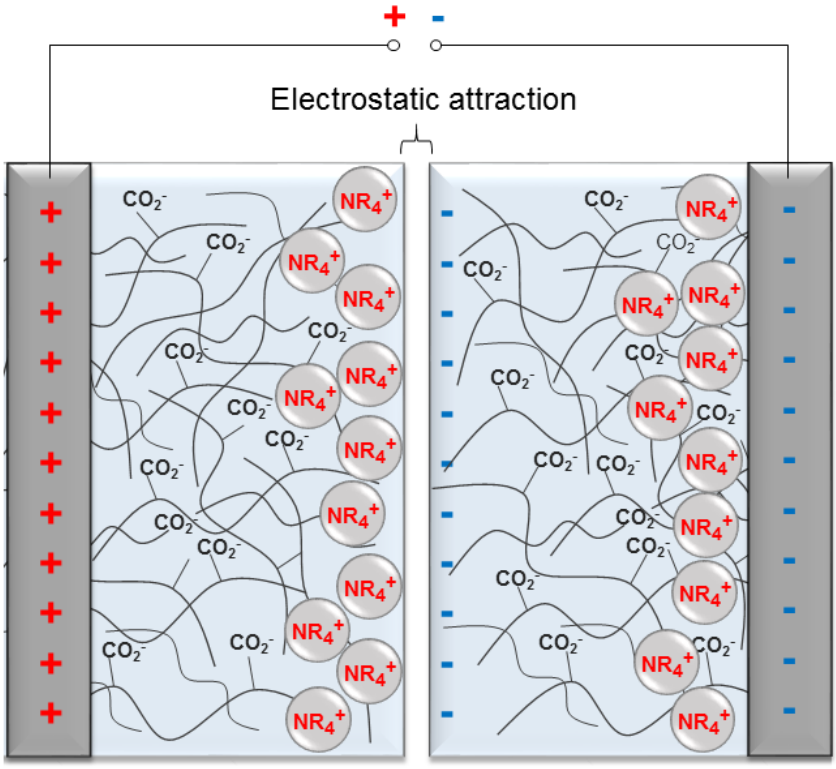

Figure 2. Diagram illustrating the migration of charge through a JR electrode/ionomer sandwich structure.

1.2 ION MOBILITY

Perhaps the most important property that influences a JR-style material's electroadhesive response is its ability to mobilize its charge carriers, such as the counterions in this work. In ion-containing polymers, this property is the ion mobility, μ, and is described by the Nernst-Einstein equation:

$$\mu = zeD/kT \qquad (4)$$

Where z is the valency of the ions, e is the elementary electric charge, k is the Boltzmann constant, T is temperature, and D is the ionic diffusion coefficient.[22] The Cohen and Turnbull equation describes the diffusion of small particles in polymers as follows:

$$D(T) = D_o \exp(-\gamma V_i^*/V_f) \qquad (5)$$

Where D_o and γ are constants, V_f is the free volume of the polymer, and V_i^* is the critical volume required for migration.[23] V_i^* is dependent on the size of the particle and its affinity for the polymer backbone, and V_f is dependent on the temperature of the system relative to its glass transition temperature.[22] In the case of the ionic polymers investigated in this work, the ion mobility only depended on the diffusion of the ion, as the valencies of the ions were consistent. The factors affecting diffusion that could have been affected by the identity of the counterion are the free volume of the polymer (influenced by the glass transition temperature change in respect to counterion identity) and the critical volume (influenced by the radius of the counterion). By changing the size of the counterion, conflicting factors are adjusted, namely that a larger ion will increase both *Vi** and *Vf*. The magnitude of each change was not measured directly, but the ion mobility could be investigated with indirect quantification.

The measurements made in this work were not direct representations of the ion mobility of the polymers, but indirect means of examining properties related to ion mobility. Glass transition temperature is directly related to ion mobility, as shown by Ohno et al.[24] As the Tg decreased in the ionic liquid based polymers, the free volume through which a mobile ion can migrate in the polymer matrix increased, therefore increasing the ion mobility of the polymer. By measuring the glass transition temperature of our ion-containing polymers, we were able to uncover the relationship between counterion size and free volume in the material. As proven by Tudryn et al, as the size of a counterion in an otherwise unchanged polymer was increased, the glass transition temperature decreased accordingly due to plasticization.[25] According to these studies, our expectation was that as the counterion size in our ion-containing polymers increased, the glass transition temperature would decrease, and thus the ion mobility would increase.

The second measurement made to attempt to investigate the ion mobility of our polymers was to determine their electrical resistivities. As the electrical resisitivity of a material is a composite of all mechanisms for transferring a charge, the material's ionic conductivity is included in this property.[26] Although the method by which we determined the electrical resistivity of each polymer was unable to decouple the components, the measure of the bulk resistivity allowed insight into the ion mobility of the materials. If all other mechanisms were equal between materials, the resistivity would decrease with an increase in ion mobility, due to a less restricted propagation of charge carriers.

1.3 INDIRECT MEASUREMENT OF ADHESION

Very little research has been performed on quantifying the effects of Johnsen-Rahbek electroadhesion on the stiffness of a structure. In the past, JR-style electroadhesion was employed for applications such as the chucking of a silicon wafer in lithography experiments without need for numerical data on the strength of the adhesion.[27,28,17] In these cases, a silicon wafer was held stationary by applying a potential across the substrate to clamp it to an electrode, leaving the active surface available for lithographic etching. As the scope of this work focused on changing the mechanical properties of constructs made by interacting layers, however, we were interested in developing methods for accurately comparing the electroadhesive properties of different polymers in geometries relevant to our objectives.

In the studies described herein, electroadhesion is characterized by comparing the mechanical stiffness of layered laminate structures. The force necessary to displace a structure consisting of stacked electrode-ionomer samples when experiencing no electroadhesion will be simply a

function of the stiffness of the material itself. Because nothing is present to bond the layers together, each layer is free to slide with respect to the other. This slipping essentially allows each layer to experience the full applied load, and thus the effective stiffness of the structure will decrease as the same sample thickness is divided into more layers.[13] However, once an electric potential is applied to induce electroadhesion, the layers will able to transfer forces between one another, causing the structure as a whole to resist stresses more efficiently (Figure 3). By comparing the rigidity of a sample under varying applied potentials, the effects of electroadhesion can be indirectly determined.

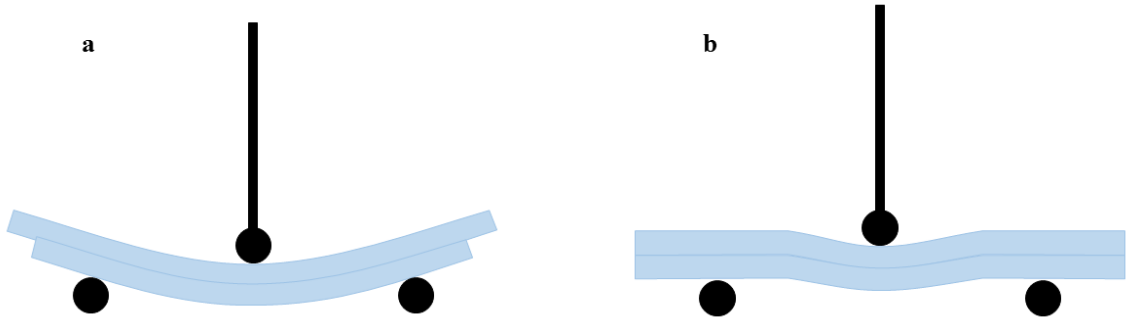

Figure 3. Comparison of a) unbonded and b) bonded layered structures.

1.3.1 Diaphragm method

A custom instrument built by collaborators in the University of Pittsburgh's department of mechanical engineering was used for preliminary experiments to measure the rigidity of a circular disc structure. Graduate student Eliot George and his supervisor Dr. William Clark fabricated the apparatus, wrote the computer code, and worked with us to establish a measurement protocol. Figure 4 illustrates the setup of the diaphragm apparatus in which a sample is deformed by a known pressure of compressed air, and the deformation is measured by an optical sensor.[29]

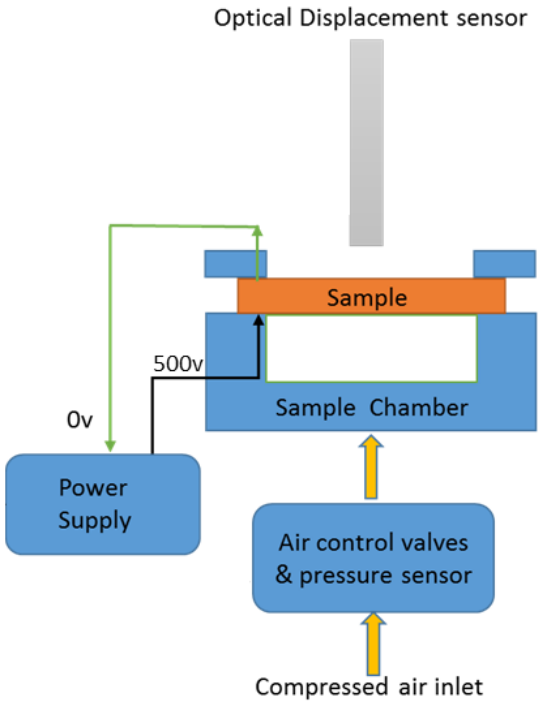

Figure 4. Schematic of circular diaphragm apparatus.

To measure electroadhesion in this apparatus, a sandwich structure composed of two electrode/polymer discs was introduced to the instrument and the effective Young's modulus of the entire sample was measured with and without exposure to an electric potential (Figure 5). The difference in modulus between the biased and unbiased samples must be the result of electroadhesion generated between the layers. By measuring the pressure of the compressed air and the resulting deflection of the discs, the effective Young's modulus of the sample was calculated via the following equations:

$$w(r) = Pa^4[1-(r/a)^2]^2/64D \qquad (6)$$

$$D = Eh^3/12(1-\nu^2) \qquad (7)$$

Where $w(r)$ is the deflection of the sample, P is the applied pressure of compressed air, a is the radius of the disc, r is the radial coordinate of measurement, E is Young's modulus, h is the thickness of the sample, and ν is Poisson's ratio of the polymer.[30] If deflection was measured at

the center of the disc, $r = 0$ and the equations can be combined and simplified to solve for Young's modulus from sample geometry and experimental results:

$$E = 12Pa^4(1-\nu^2)/64w(r)h^3 \qquad (8)$$

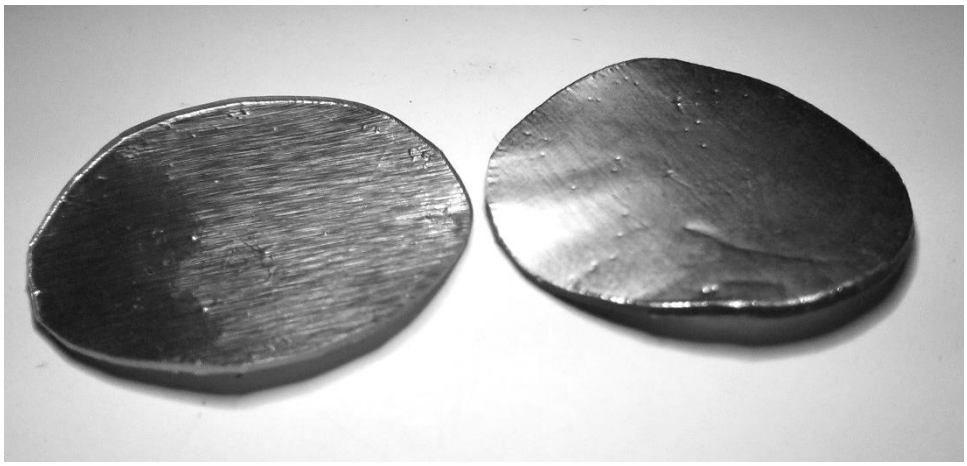

Figure 5. Aluminum electrode/polymer disc samples. Left sample is ionomer layer up, right sample is electrode layer up.

1.3.2 Three-point bending method

Most reports on the investigation of electroadhesion's effect on mechanical properties involve the use of a variable modulus cantilever beam.[15,16,14] In this case, one end of a composite rectangular beam is fixed while the other end is free. A load is applied to the free end and the deflection is measured. We chose instead to use a three-point bending apparatus in which both ends of the structure remain unfixed, because it allows maximum ease of displacement between the unadhered layers and because the method is quite commonly used to probe the rigidity of a beam structure.[31,32] A sample with a rectangular beam geometry is supported on either end and the center is displaced at a constant rate. The force required to displace the center of the beam a

certain distance is measured and the effective flexural modulus of the material is determined by the equation:

$$E_f = L^3 m / 4bd^3 \qquad (9)$$

Where E_f is the flexural modulus, L is the length of the beam, m is the slope of the linear portion of the force vs. displacement curve, b is the width of the beam, and d is the thickness of the beam. In this experimental setup, the ends of the beam remain unfixed so as to have freedom to slide with respect to one another. This geometry allows for the greatest difference in rigidity between an adhered versus adhesion-free state.

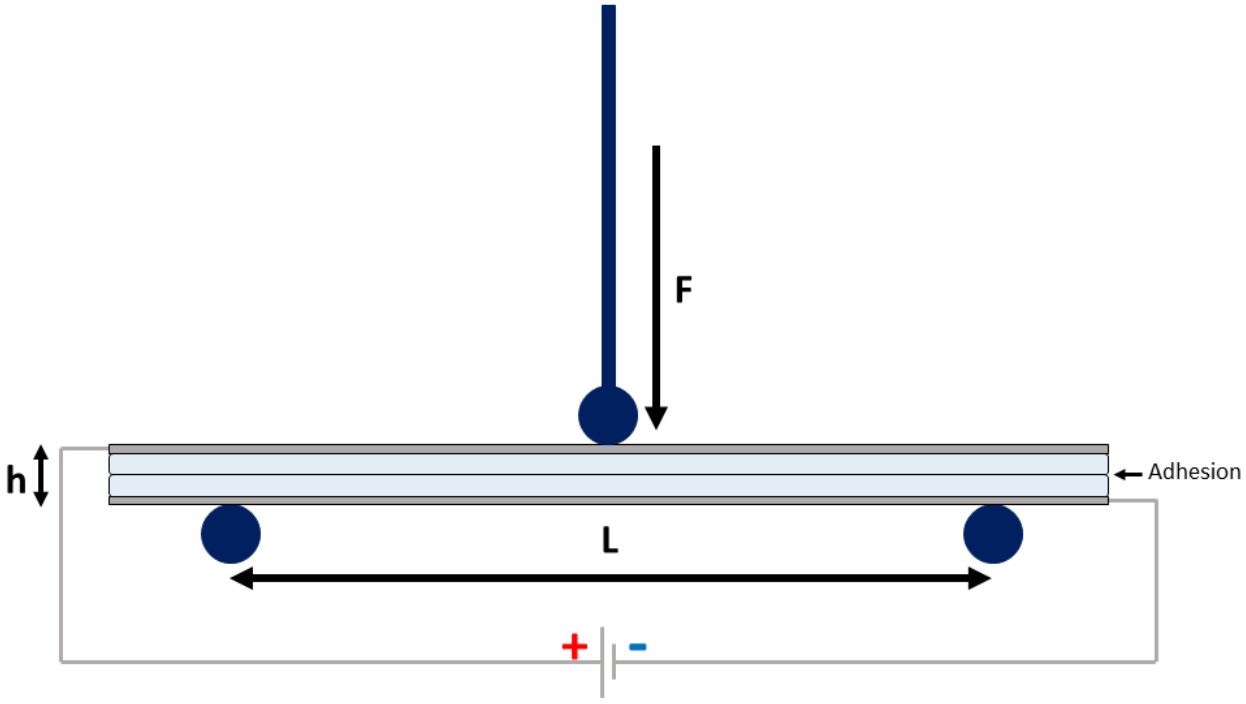

Figure 6. Diagram of three-point bending apparatus

A three-point bending apparatus was built in collaboration again with George and Clark from the mechanical engineering department at the University of Pittsburgh. A load-cell attached to a crosshead was controlled by a computer and could be raised and lowered at a constant rate. The

entire instrument was enclosed in a chamber that could be purged with nitrogen to provide a controlled atmosphere for testing. The sample geometries were kept as consistent as possible to ensure any differences were due to the material rather than a different physical geometry and to keep force measurements in the correct regime for the instrument.

1.3.3 Preliminary Results and Material Design

In a 1996 patent authored by Cipriano and Longoria, a number of electroresponsive polymer materials were listed as exhibiting electroadhesive properties.[33] Of these, the only polymer seemingly suitable for JR-style applications was a derivative of poly(ethylene-*co*-acrylic acid) made by suspending the PEAA in an aqueous basic solution of a tetramethylammonium salt. Upon neutralization with this quaternary amine, the polymer proved to be electroadhesive.

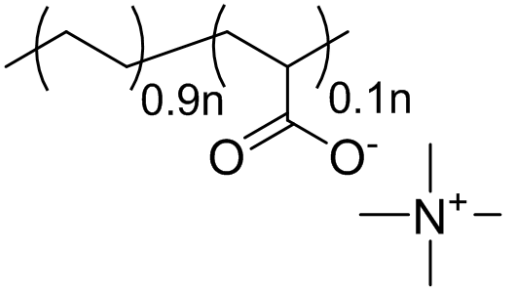

Figure 7. Structure of tetramethylammonium neutralized poly(ethylene-*co*-acrylic acid), PEAA-TMAH.

Preliminary experiments were performed using this same material in the diaphragm apparatus, and promising results were obtained. Undergraduate researcher Nicole Bauer in collaboration with graduate student Jeffrey Auletta fabricated electrode/polymer composite discs for use in the apparatus, and provided the proof of concept necessary for pursuing the research depicted herein. While the experimental technique involving the diaphragm apparatus proved sufficient for

preliminary procedures, the full extent of adhesion was masked due to the physical requirements of the instrument. In order for the sample to experience the full force of the pressurized air, the sample needed to form a gas-tight seal around the sample chamber. The act of clamping the perimeter of the sample with an O-ring achieved this goal, but also limited any potential change in rigidity of the sample. Under no electroadhesive force, the material should exhibit a much lower effective Young's modulus due to the ability of the sample layers to slide in respect to one another compared to when the layers are electrostatically bound. Clamping the perimeter of the disc greatly reduced the possibility of relative motion, and thus the resultant change in effective modulus was not a complete description of the material's response to the electric field. Nevertheless, Bauer determined that the PEAA-TMAH disc samples exhibited a modest increase in Young's modulus when exposed to 500 V, corresponding to the presence of electroadhesion. This positive preliminary result prompted the continuation of the study and more thorough characterization of the material.

With positive preliminary results obtained, attention could be directed to developing the library of materials that exhibit the JR force of interest. To investigate the chemistry involved in these ionomer materials, a study on the structure-activity relationship of counterion identity to JR response was prepared. As the electroadhesive response of PEAA-TMAH had been confirmed, a series of PEAA based ionomers containing other tetraalkylammonium cations were synthesized. By utilizing species from the same family of counterions, such as tetraethylammonium and tetrapropylammonium, the variables were limited primarily to ionic size and hydrophobicity. In collaboration with Auletta; PEAA-TMAH, PEAA-TEAH, and PEAA-TPAH were all prepared via the same synthetic methods and subjected to the same characterization techniques, the results of which are presented herein.

2.0 RESULTS AND DISCUSSION

2.1 EXPERIMENTAL APPROACH

Since the JR force depends variably on the effective voltage of the electric field, any change to the ability of a material to produce a more prominent charge at the interface between layers should affect the resulting force. The objective of the research reported herein was to determine how the identity of the counterion in these ionomer materials affects the difference in effective flexural modulus between charged and uncharged states. The difference in modulus due to interlayer adhesion should depend on a number of factors such as ion mobility, electrical resistivity, and elasticity. Each of these facets should be influenced by the identity of the counterion and will be measured directly or indirectly in this report. Glass transition temperature is inherently related to ion mobility because increased free volume in the polymer facilitates ion movement.[24,34] By measuring the change in T_g, the ion mobility of each material can be indirectly compared. The electrical resistivity of the material directly influences the JR force by altering the effective voltage, V_{eff}, at the interface. Electrochemical impedance spectroscopy was utilized to determine the bulk resistivity of the ionomers. Intrinsic elastic modulus of each material gives insight into the rigidity of the "off" state of the electroadhesive structures, so a standard tensile testing technique was used to measure the tensile modulus of the ionomers. While each sample was conditioned at a constant humidity prior to all measurements, the

ionomers potentially demonstrated differing water contents. To eliminate concerns of water's effect on electroadhesion, the water uptake of the materials was measured. Finally, the electroadhesion produced in electrode/ionomer sandwich structures was indirectly measured by determining the effective flexural modulus of the samples at various applied potentials.

2.2 THERMAL PROPERTIES

Thermal properties, such as glass transition temperature of the material, were expected to influence the electroadhesive response of the ionomer materials as they affect the ionic conductivity of the sample. Differential scanning calorimetry (DSC) thermograms were obtained for PEAA and each ionomer to compare the effects of the counterions. Prior to testing, samples were dried in a vacuum oven at 40 °C for 24 h. This procedure ensured that a negligible amount of water was present in the samples, and the profile of the heating and cooling curves would be unaffected by the phase changes of water. The DSC experiment consisted of two heating and two cooling cycles, from -20 to 70 °C at 10 °C/min. The crystallization temperature (T_c), if present, was calculated from the first cooling cycle, and the glass transition temperature (T_g) was determined from the second heating cycle.

Table 1. Summary of experimental results

Material	T_g	T_m	T_d	Water content	ρ^c	E^e	E_f at 0V	E_f at 450V	Modulus change[f]
	°C[a]	°C	°C	Mass %[b]	MΩ·cm	MPa	MPa	MPa	
PEAA	39	80	-----	-----	10^{10} [d]	38.1	80.7	71.7	89%
PEAA-TMAH	43	-----	140	12.2	0.28	11.0	71.5	107	154%
PEAA-TEAH	39	-----	120	11.0	0.69	2.92	43.1	86.1	200%
PEAA-TPAH	37	-----	115	9.6	1.55	0.99	30.4	74.1	244%

[a] Determined from half Δc_p. [b] Mass of water relative to mass of polymer backbone. [c] Volume resistivity. [d] Young's modulus. [d] Literature value.[35] [e] Calculated by dividing flexural modulus at 450 V by flexural modulus at 0 V.

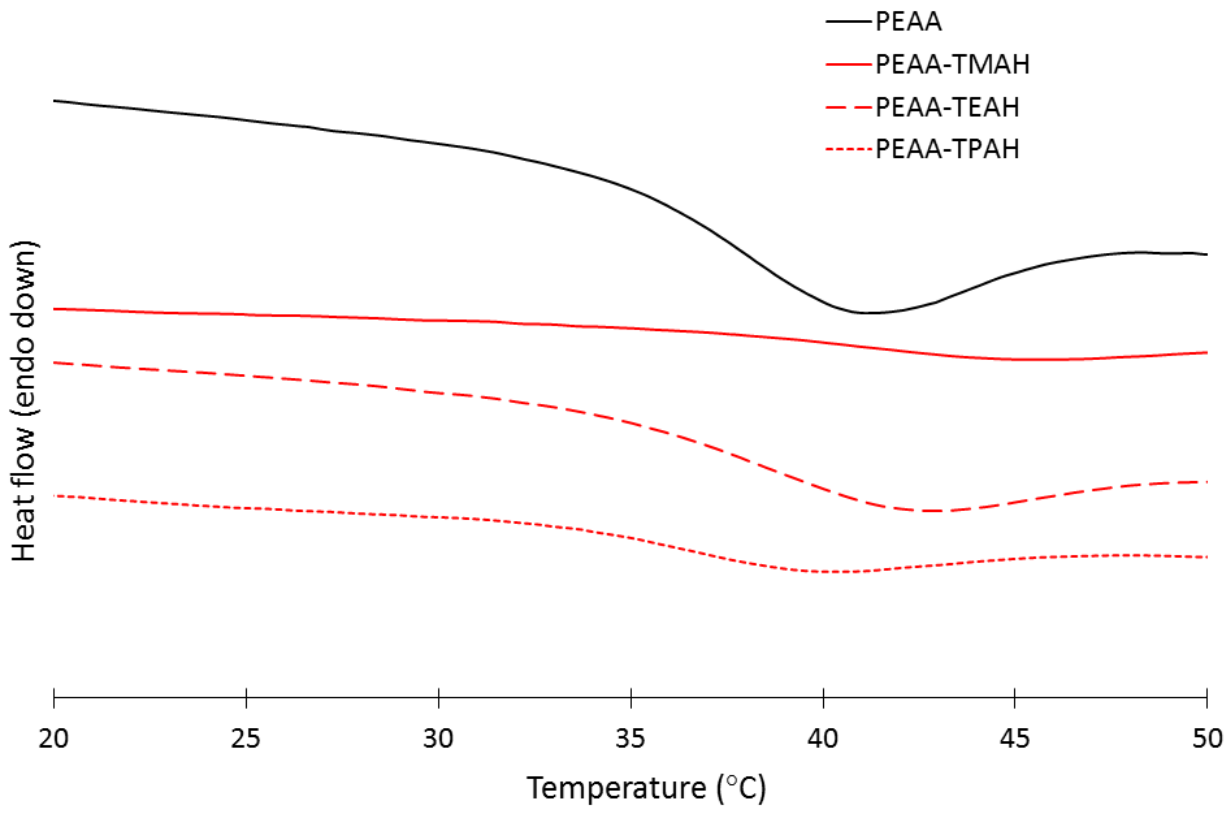

Figure 8. Second heating cycle of DSC thermograms**.**

PEAA's T_g initially increased from 38.4 °C to 42.6 °C upon neutralization with TMAH, and decreased upon elongation of the alkyl chains to 39.2 °C and 36.9 °C for TEAH and TPAH respectively (Figure 8, Table 1). The T_g of virgin PEAA is consistent with values reported in the literature.[36,37] The increased T_g for the TMAH counterions is somewhat surprising as it would generally be expected that the larger counterion would increase free volume in the polymer. However, in a study on comparable acrylate ionomers, Hirasawa et al. observed a similar trend in the glass transition temperature: the T_g increased upon deprotonation of the virgin polymer in the presence of bulky counterions.[38] We hypothesize that the while the strong hydrogen bonds present in the virgin PEAA are lost in the TMAH-derivative, the intrachain bonding due to the formation of ionic aggregates is sufficiently large to compensate. With the increase in alkyl chain lengths seen in TEAH and TPAH derivatives, however, aggregation is diminished and the larger size of the ions produce the expected decrease in T_g.[39]

The prominent exothermic peak in the cooling curve of PEAA is an indication of the crystallization of ethylene units in the polymer backbone (Appendix).[36] Upon deprotonation, all evidence of crystallization is lost, and the resulting ionomer is clearly amorphous. The likely cause of the lack of crystallinity is the disruption in the packing of ethylene segments by the bulky counterions. The ionic radii of each alkylammonium cation is sufficient to prevent the polymer backbone from assembling into crystalline domains.

Thermogravimetric analysis (TGA) was also performed on the materials in order to determine the likelihood of sample degradation at the working temperatures of the electroadhesion experiments. Again, samples were dried *in vacuo* at 40 °C to reduce the signal from the loss of water. Each sample was heated from 20 to 200 °C at 2 °C/min and the relative mass was measured (Figure 9).

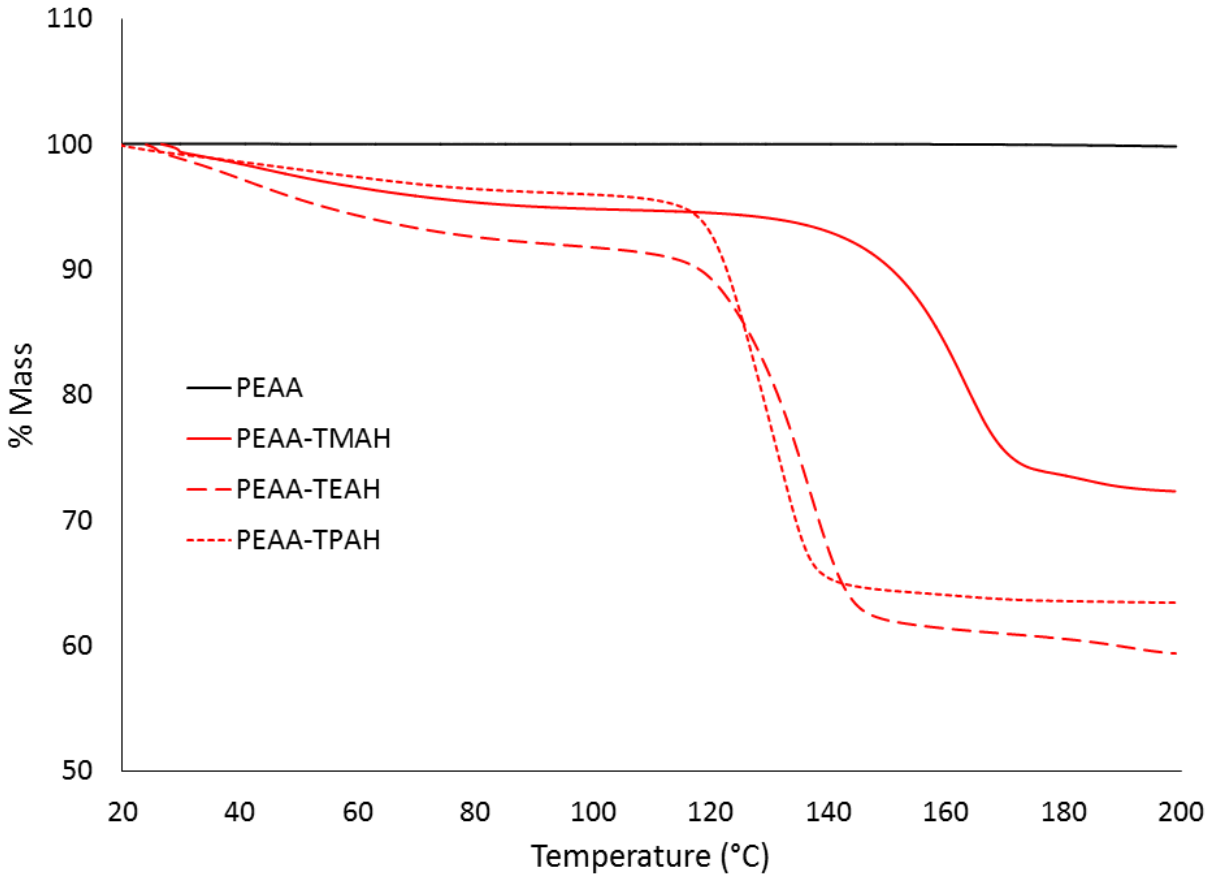

Figure 9. TGA mass loss plots for PEAA materials.

As expected, PEAA showed virtually no change in mass upon heating, as there are no labile species in the material. The ionomer samples were less thermally stable, decomposing to form amines above 100 °C. Decomposition for PEAA-TMAH occurred at around 140 °C, while T_d for PEAA-TEAH and PEAA-TPAH were approximately 120 °C. The reason for PEAA-TMAH's slightly higher thermal stability is unclear, but is potentially due to either the binding energy of the counterion to the polymer backbone or the stability of the product amine. If tetramethylammonium ions are more tightly bound to the polymer backbone, a higher activation energy would be required to break those interactions. Similarly, if the product of decomposition

for PEAA-TMAH is less stable than that of PEAA-TEAH and PEAA-TPAH, the decomposition would be less favored at the same temperatures.[40] The results obtained from TGA granted the confidence that these materials would experience no unexpected physical changes due to heating during experimentation, as decomposition temperatures were all above 100 °C. Once the thermal stabilities of these ionomers were confirmed, the analysis of their electrical conductivities could be performed.

2.3 ELECTRICAL PROPERTIES

Electrochemical impedance spectroscopy (EIS) is a commonly used technique for elucidating the bulk electrical properties of polymer materials.[41] EIS was employed to determine the electrical resistivity of the ionomer materials, as this property influence the effective voltage of the electric field produced in electroadhesion experiments. A small potential is applied across a range of frequencies, and the response of the polymer was measured by the instrument. As the polymer attempts to accommodate the applied potential, the measured current is affected by the reactance (the imaginary portion of the impedance caused by the storage of charge due to capacitance) and the normal electrical resistance (the real portion of the impedance) of the material. The impedance causes a lag in the electrical response of the polymer, which produces a phase angle between the sinusoidal applied potential and the measured current. In a frequency range dictated by the identity of the material, the polymer enters a frequency-independent regime in which the impedance is solely a product of the electrical resistance. The simplest model for the impedance of a polymer is a parallel circuit consisting of a resistor modeling the resistance and a capacitor modeling the reactance.

Samples were fabricated by hot pressing a disc of ionomer between two circular electrodes (Figure 10). The resistance of the sample was determined by sweeping the frequency of the applied potential from 25 kHz to 100 kHz and fitting the Nyquist plots in Figure 11b to an equivalent circuit consisting of a capacitor and a resistor. The physical dimensions (thickness *h* and diameter *d*) were measured and used to calculate the bulk resistivity of the material from the measured resistance.

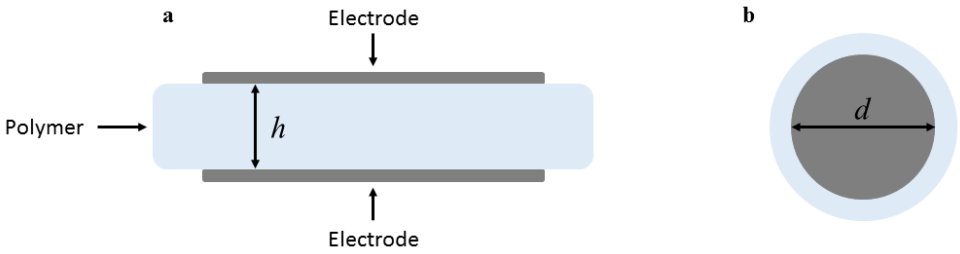

Figure 10. Samples for EIS measurements a) cross-sectional view, b) top-down view.

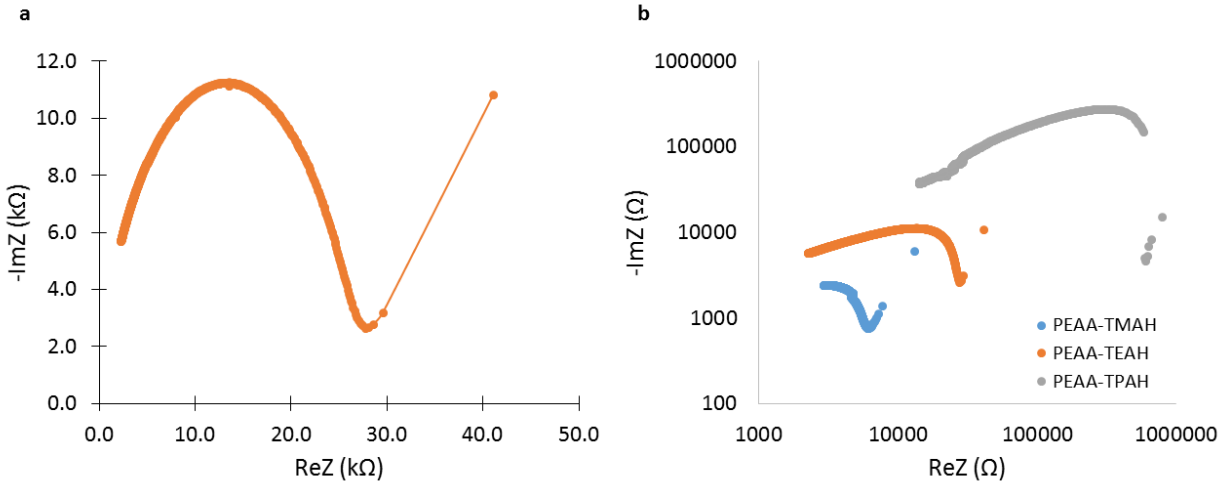

Figure 11. Nyquist plot for a) PEAA-TEAH and b) PEAA-TMAH, PEAA-TEAH, and PEAA-TPAH.

The resistivity of the material can be calculated from impedance spectroscopy data using one of two methods. First, the resistivity at each frequency can be calculated by the equation:

$$\rho(f) = (A\,|Z(f)|)/(h\cos\theta(f)) \qquad (10)$$

Where A is the electrode area, h is the sample thickness, $|Z(f)|$ is the complex impedance $((Z_{real})^2+(Z_{imaginary})^2)^{1/2}$ at the given frequency, and $\cos\theta(f)$ is the phase angle at the given frequency. By plotting resistivity versus frequency, a plateau signifying the frequency-independent regime of the material impedance can be equated to the bulk resistivity of the polymer. The second method involves fitting the obtained Nyquist plot (reactance vs. resistance) to the equivalent circuit of a resistor and capacitor in parallel. By extrapolating the high-frequency portion of the curve to intersect the X-axis, the contribution of the reactance to the complex impedance can be eliminated ($Z_{imaginary} = 0$) and the bulk resistivity can be approximated as the X-intercept.[26]

The polymers' electrical resistivity trended with an increase in counterion size. TMAH, TEAH, and TPAH neutralized PEAA exhibited bulk resistivity values of 0.28, 0.69, and 1.55 MΩ·cm respectively with less than 2% error in the fitted curve. Additionally, the capacitance of each ionomer was determined by the same model and were all roughly the same (PEAA-TMAH = 140 pF/cm^2, PEAA-TEAH = 114 pF/cm^2, PEAA-TPAH = 135 pF/cm^2). Because the resistivity values were not determined in the frequency-independent regime (typically >1 MHz), the absolute resistivities are not exact representations of the material property due to the need for extrapolation. However, the Nyquist plots were all modeled with less than 2% error in the fitted curve, indicating that the calculated bulk resistivities are excellent approximations, and a clear trend is present between resistivity and counterion size. The resistivity of each ionomer is appropriate for JR-type electroadhesion, while PEAA's previously reported resistivity of >10^4 MΩ·cm is outside the range required to observe JR forces.[35] In comparison, typical materials used for coulombic-style applications such as ceramics (aluminium nitride and boron nitride, ρ =

10^7–10^8 MΩ·cm)[42,43] and dielectric polymers (poly(vinylidene fluoride), ρ = 5x10^8 MΩ·cm)[44] are many orders of magnitude more resistive than even PEAA-TPAH. The capacitance of the ionomers is comparable to the most common polymer capacitor, polypropylene, which exhibits a capacitance between 50 pF/cm^2 and 5 μF/cm^2.[45]

The cause of the direct trend between counterion size and resistivity cannot be explained by any one mechanism of electrical conductivity because the measured impedance of the materials is a composite of all mechanisms of propagating a charge, such as ion mobility and electron conductivity. While a larger counterion increases the free volume of the polymer and decreases the T_g, the longer alkyl chains also increase the amount of interactions with polymer backbone and could decrease the ion conductivity. Additionally, a larger ion will sterically block the conduction pathways of electrons through the material and result in more resistive polymers, as has been shown to be the case in solid-phase polyelectrolytes by Kimpton et al.[46] Regardless of the weight of the contributions from each of these factors, the bulk resistivity could be concluded to increase along with counterion size.

In order to determine if the cause of the difference in resistivity is truly the size of the counterion and not due to differences in water-uptake of the ionomers, a water content study was performed. As the measured value defines the electrical conductivity of the sample, the amount of water present could be of importance. Although each sample was conditioned by storage in a container maintained at 11% relative humidity, the actual water content of the sample varied depending on the relative hydrophobicity of the material. As the length of the counterion alkyl chains grows (ionic radius of TMA^+ = 0.28 nm, TEA^+ = 0.34 nm, TPA^+ = 0.38 nm),[47] the ion becomes more hydrophobic. Whether this slight difference in affinity for water affects the bulk

material property was determined by measuring the difference in mass between a “dry” and “wet” ionomer.

A sample of each ionomer was heated at 60 °C under vacuum for a week to ensure a completely dry sample. A dry mass was obtained and the mass of polymer backbone was calculated. The copolymer as purchased was 20 wt.% acrylic acid units, and assuming a complete neutralization by the alkylammonium bases (1:1 mole ratio of AA to counterion), the mass of the counterions could be subtracted in order to normalize the “dry” mass to be strictly the mass of the polymer backbone. The ionomers were then transferred individually to a container maintained at 11% relative humidity for five days to allow for equilibration. The change in mass after equilibrating in the controlled humidity chamber was defined as the total mass of water in the sample, and thus the water content was calculated by:

$$\text{Water Content} = \Delta m/m_b \times 100\% \qquad (11)$$

Where Δm is the change in mass attributed to water, and m_b is the mass of the polymer backbone. The water content for samples conditioned at 11% was determined to be only slightly dependent on counterion identity. Each ionomer differed by approximately 1 mass percent, with PEAA-TMAH, PEAA-TEAH, and PEAA-TPAH containing 12.2 %, 11.0 %, and 9.6 % water respectively. While these water contents differed slightly, the effect of water on the material properties was inconsistent. For example, a lower water content should have resulted in a less swollen ionomer, and thus a higher T_g. However, PEAA-TPAH exhibited the lowest T_g and lowest water content. Contrary to the effect on T_g, a higher water content did correlate with a lower resistivity. Due to these conflicting trends relative to water, the properties of the materials were concluded to be a function of counterion identity and not strictly water content.

2.4 MECHANICAL PROPERTIES

Once the ionomers were confirmed to be applicable to JR force measurements, the effects of PEAA neutralization on the elastic modulus could be measured. Dogbone samples were subjected to a typical tensile elongation test. Each material was stretched at a constant rate and a stress vs. strain curve was obtained. From the stress vs. strain curve, the Young's modulus of the polymer could be calculated from the equation:

$$E = FL_0 / A_0 \Delta L \qquad (12)$$

Where E is the Young's modulus, F is the applied extensional force, L_0 is the initial gauge length, A_0 is the cross-sectional area, and ΔL is the elongation of the sample. The results of the experiments resembled a typical viscoelastic material, with a linear region of elasticity followed by a viscous plateau as a result of stress relaxation.[48] Moduli were calculated from the linear portion of the curve to ensure an accurate description of the elastic properties of the material.

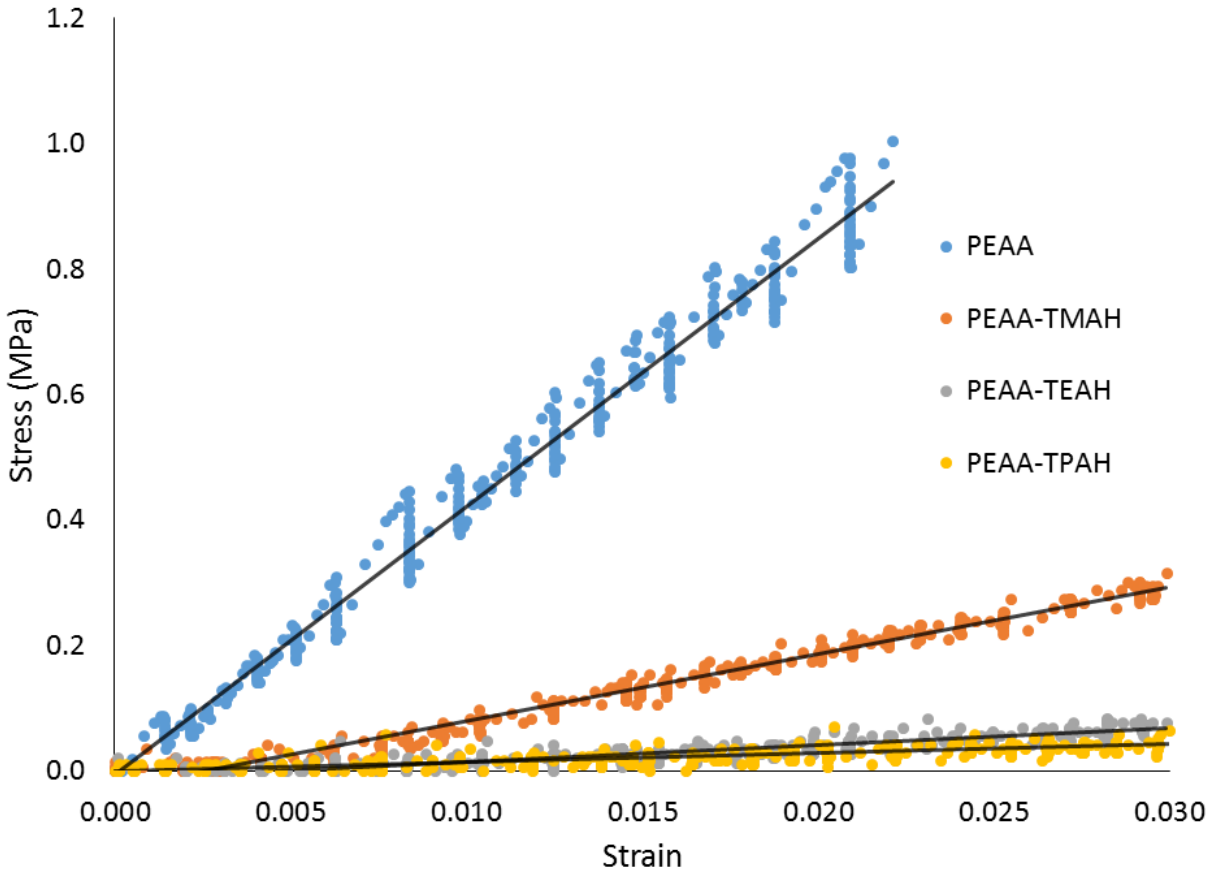

Figure 12. Linear portion of stress-strain curves for PEAA and ionomers.

PEAA exhibited a modulus of approximately 40 MPa, which dropped substantially upon deprotonation with tetraalkylammonium base. The decrease in modulus varied proportionally with size of the counterion, with PEAA-TMAH, PEAA-TEAH, and PEAA-TPAH possessing Young's moduli of 11.0, 2.9, and 1.0 MPA, respectively. Prior to neutralization, PEAA contains crystalline domains, as confirmed by DSC measurements. These crystalline regions result in a stronger material due to their resistance to physical deformations.[48] Upon deprotonation, these crystalline domains are eliminated, explaining the significant drop in mechanical properties. The inverse trend of alkyl chain length to Young's modulus is a result of plasticization of the material. As the ions grow in size, they prevent efficient packing and produce a more plastic

polymer. These results are as expected from the thermal properties of the ionomers, as a decrease in T_g correlates to a more plasticized and thus less elastic material.

2.5 ELECTRORESPONSIVE STRUCTURE STIFFENING

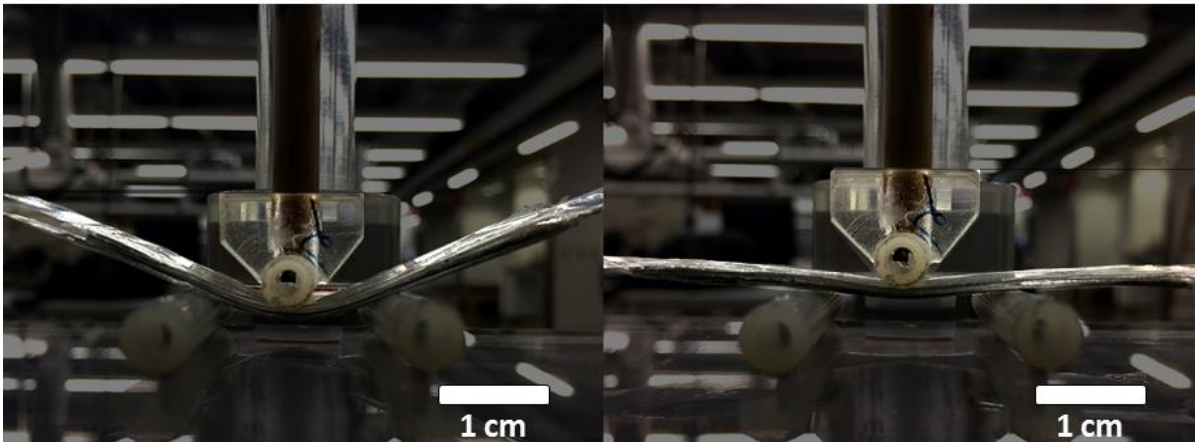

Figure 13. PEAA-TMAH sandwich structure under the same pressure, uncharged (left) and charged (right).

The effective flexural modulus, which is a function of the adhesion between the polymer layers, was measured using a custom three-point bending apparatus and was found to depend on the identity of the counterion and the applied potential. Consistent with the expected effects of plasticizing the material, the zero voltage flexural modulus decreased with alkyl chain length of the ammonium ion. Upon applying a potential to the system, no significant change is initially observed, with effective flexural moduli remaining rather consistent over the first few hundred volts. An inflection point occurred around 250-350 V, with the effective moduli sharply increasing with applied voltage. The samples suffered dielectric breakdown at potentials greater than 450 V for all of the polymers under the experimental conditions. Measured leakage currents were observed to decrease as counterion size increased.

At 450 V, the neutralized ionomers exhibited dramatic stiffening whereas the virgin PEAA sandwich structure retained its initial rigidity. The effective modulus at 450 V for PEAA-TMAH was 36 MPa higher than at 0 V, resulting in a charged modulus 150% that of its uncharged modulus. PEAA-TEAH's modulus increased by 43 MPa when biased, yielding a charged modulus 200% as stiff as when under no applied potential. Similarly, PEAA-TPAH exhibited an increase of 44 MPa over its uncharged modulus when subjected to 450 V. Due to its lower uncharged modulus, this response corresponded to a charged modulus 250% that of its uncharged modulus.

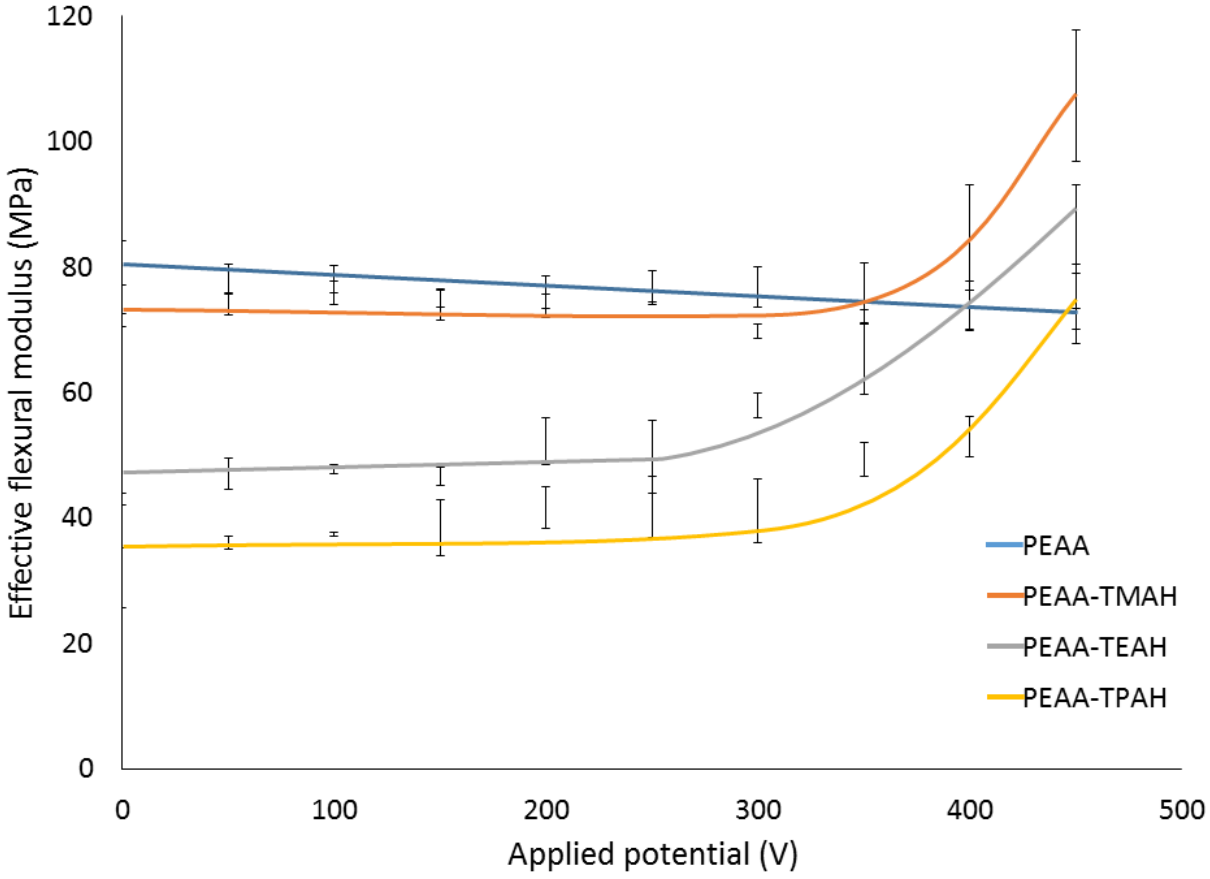

Figure 14. Effective flexural moduli of ionomer sandwich structures at various applied potentials. Trend lines were added for clarity. Error bars reflect the standard deviation across three trials.

A clear trend in the relative effective modulus increase is present as the size of the counterion becomes larger. As the glass transition temperature decreases, the flexural modulus of the samples under no potential decreases accordingly. This drop in initial flexural modulus provides for a softer "off" state from which the structure may be stiffened, resulting in the possibility for a larger delta between on and off states. The lower glass transition temperature also allows for more free volume through which the mobile charge carriers can migrate, increasing the effective charge at the interface. This more efficient build-up of charge at the interface, when combined with the lower leakage current associated with a higher electrical resistivity, results in a greater effective voltage at the interface. As the JR force depends on the effective voltage, these factors correlate to a higher adhesive force and therefore a greater stiffening of the structure.

3.0 CONCLUSIONS

3.1 RESEARCH SUMMARY

The cumulative results from the research presented herein is compiled in Table 1. A clear trend for each property related to the identity of the counterion is evident. Thermally, a larger counterion resulted in an ionomer with a lower glass transition temperature due to the increase of free volume of the material, while also exhibiting a lower decomposition temperature due most likely to the stability of the products of decomposition. The water content of the ionomer decreased as the material became more hydrophobic, but remained within about 1% of each other. Electrical resistivity decreased substantially upon deprotonation, but increased with ion size due to physical electron blocking. As a result of plasticization, ionomers with larger counterions were less elastic than those with smaller counterions. An inverse trend between ion size and flexural modulus is present both at 0 V and at 450 V, however due to the larger drop in uncharged modulus compared to the charged modulus, the overall modulus change increases as the counterion size increases.

3.2 FUTURE WORK

Following the results of the research presented in this work, future studies could proceed in a number of directions. The materials investigated in this work have all been polyanions, that is, the charge located on the polymer backbone is negative and the counterions within have positive charges. Polycations are polyelectrolytes that have the opposite distribution of charges, with anionic counterions and positive charges attached to the polymer matrix. Polymerized ionic liquids (PILs) make up a specific class of polycation that has received attention recently. Typical imidazolium, pyridinium, or phosphonium ionic liquids have been functionalized with terminal olefins which allows for the polymerization or copolymerization of these positively charged species.[49] Imidazolium-based PILs can be readily synthesized by quaternizing an imidazole with an alkyl halide.[50,51] These PILs have been shown to exhibit properties that are promising for a material compatible with the JR effect, such as low T_g and high ionic conductivity.[52,53]

Ionic liquid polymers are especially appealing for future research into electroadhesive structures due to the ability to tune multiple aspects of the material. The polymer backbone itself can be altered according to the length and branching of the alkyl chain used to quaternize the imidazolium unit. For instance, a similar study to the one discussed in this report could be performed on a series of PILs with differing alkyl R groups. In addition to this, the ionic liquid monomers could be incorporated into a copolymer containing a non-ionic monomer. By adjusting the monomer ratios, the ionic density of the polymer could be tuned and its effect on the JR force could be investigated. Finally, in a similar fashion to the PEAA-based ionomers, the identity of the counterion could be changed to again determine how the properties of the material depend on the ions contained within. The combination of all of these tunable factors makes the prospect of PIL ionomers an exciting direction for this research to continue towards.

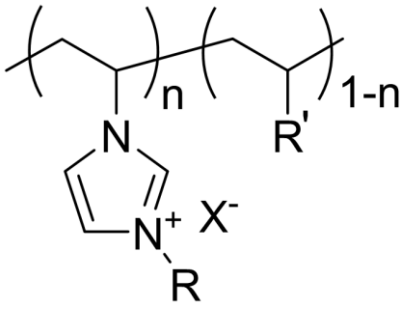

Figure 15. General structure of an imidazolium poly ionic liquid.

In addition to possessing multiple variable functionalities for chemical optimization, discovering polycationic ionomers that experience the JR effect has another purpose for continuing the research presented herein. An evident drawback to the PEAA-based ionomer system is that the only mobile charge-carrying unit is the positively charged tetraalkylammonium cation. When the structure is charged, the ionomer layer affixed to the anode builds up a positive charge at its surface due to an accumulation of cations. However, while the ionomer layer cast onto the cathode will experience the same migration of charge, it will not be accumulating a high concentration of charge at the surface. Instead, the surface will exhibit a local effective negative charge due to the absence of positive counterions. This effective negative charge is apparently strong enough to induce electrostatic adhesion between layers, but is not of an equivalent magnitude to the positively charged surface. If a structure could be fabricated with a PEAA-based polyanion fixed to the anode and a PIL-based polycation fixed to the cathode, the surface of either layer will become charged due to an accumulation of mobile ions. This should potentially exhibit the largest effective electric field across the sample, and thus should maximize the generated JR force.

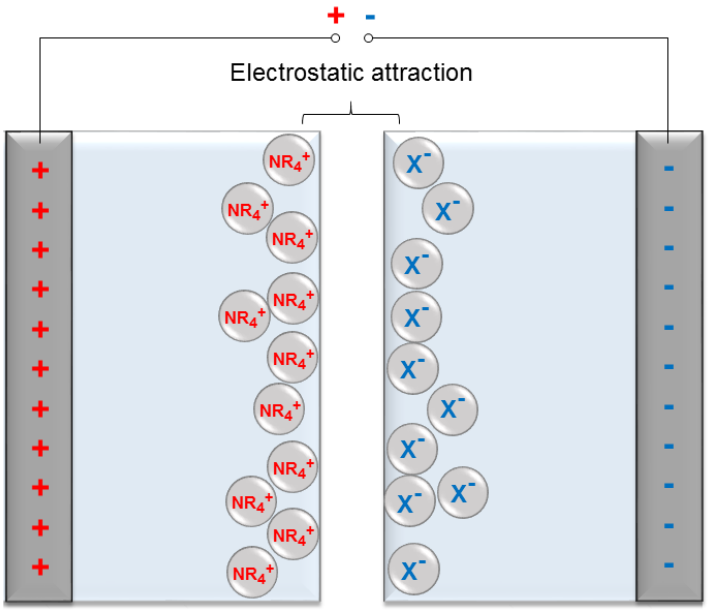

Figure 16. Theoretical structure combining PEAA-based and PIL-based ionomers.

4.0 EXPERIMENTAL

4.1 IONOMER DEPROTONATION

A typical neutralization was carried out following a procedure adapted from Cipriano and Longoria (Scheme 1).[33] PEAA (10.0 g, 27.8 mmol AA) and an aqueous solution of tetramethylammonium hydroxide (25% w/w, 10.2 g, 28.0 mmol TMAH) were combined in a round-bottom flask. To the flask, 100 mL of dH_2O was added and the mixture was stirred and heated at 70 °C until the PEAA beads dissolved, indicating neutralization of the acrylic acid was complete (about 12 h). The solution was concentrated in a hot water bath to a final concentration of about 250 g/L. Neutralizations with TEAH and TPAH proceeded similarly.

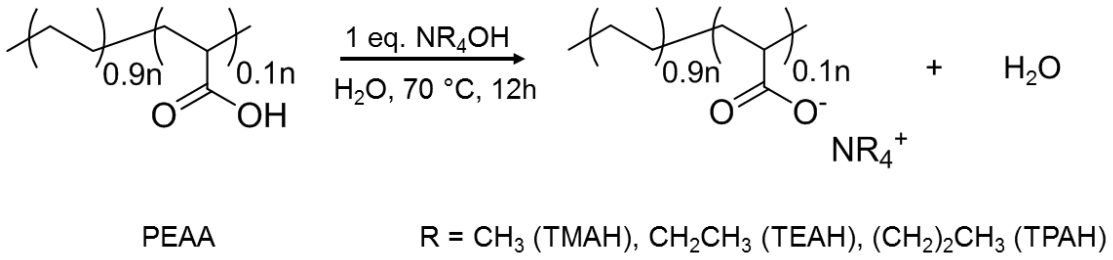

Figure 17. Neutralization of PEAA with tetraalkylammonium hydroxide.

4.2 SIZE-EXCLUSION CHROMATOGRAPHY

Relative molecular weight of unneutralized PEAA was determined on a Waters Gel-Permeation Chromatograph with a Waters 2414 refractive index detector. PEAA was dissolved in THF at a concentration of about 1 mg/mL and was filtered prior to injection. 100 uL was injected into the column and the resulting molecular weight was calculated according to a polystyrene standard (1-500 kDa). The weight average molecular weight of PEAA was determined to be 41 kDa.

4.3 DIFFERENTIAL SCANNING CALORIMETRY

Thermal properties of each polymer were evaluated by differential scanning calorimetry. About 4 mg of polymer was conditioned to dryness in a vacuum oven kept at 50 °C. The sample was transferred to an aluminum DSC pan and hermetically sealed to prevent the uptake of water. The sample was subjected to two heating cycles from 0 °C to 70 °C at 10 °C/min and the glass transition temperature was determined from the second heating cycle. Measurements were performed on a Perkin Elmer DSC 6000 calibrated with indium metal.

4.4 THERMOGRAVIMETRIC ANALYSIS

Thermal degradation data was collected on a TA Instruments TGA Q500. Approximately 15 mg of sample was dried in a vacuum oven and loaded into a tared platinum pan, in which the percent

mass change was measured over the course of each run. The temperature was ramped from 20 °C to 200 °C at 2 °C/min under a constant flow of nitrogen (60 mL/min).

4.5 SAMPLE CONDITIONING

Unless otherwise noted, prior to measurements each sample was conditioned in a chamber held at 11 % relative humidity. A solution of saturated LiCl exhibits a vapor pressure that produces a relative humidity of 11 % under a proper surface area to chamber volume ratio.[54] Each sample was stored in a sealed chamber with a saturated LiCl solution for at least three days to ensure water equilibration.

4.6 WATER CONTENT

Approximately 0.3 g of ionomer was dried in a vacuum oven at 40 °C for 3 days. A dry mass was obtained, and the sample was transferred to a chamber containing a saturated LiCl solution (relative humidity = 11 %).[54] This dry mass was a combination of the masses of ethylene units, acrylate units, and counterions. The copolymer as purchased was 20 wt.% acrylic acid, and the ratio of counterion to acrylate moiety was assumed to be 1:1. Therefore, the total dry mass could be expressed by the following equation:

$$\text{Dry mass} = (5 + MM_{ion}/MM_{acrylate}) * m_{acrylate} \qquad (13)$$

Where MM_{ion} is the molar mass of the counterion, $MM_{acrylate}$ is the molar mass of an acrylate unit, and $m_{acrylate}$ is the mass of the acrylate content of the polymer backbone. The mass of the

polymer backbone was then calculated by multiplying $m_{acrylate}$ by 5. The samples were equilibrated after 5 days (no further significant changes in mass) and a "wet" mass was obtained. The percent mass of water was determined by dividing the change in mass by the total mass of polymer and water.

4.7 IMPEDANCE SPECTROSCOPY

Samples for impedance measurements were fabricated by first drop casting a free-standing polymer film on a glass plate. The film was hot pressed between two pieces of 1 cm square aluminum shim stock to yield a sample with known cross-sectional area and thickness. Prior to analysis, each sample was conditioned in a 11 % relative humidity chamber for three days. The sample was analyzed using an Agilent 42941A impedance probe over a range of 25 kHz to 100 kHz and the resistivity was calculated by fitting the high-frequency curve in EIS Spectrum Analyser.

4.8 YOUNG'S MODULUS

The elastic modulus of each polymer was determined using an ADMET MTESTQuattro mechanical tester in the tensile mode. Dog bone samples of a drop cast film complying with ASTM D638 – Standard Test Method for Tensile Properties of Plastics were elongated at a constant rate and the tensile modulus was calculated from the first three strain percent of the linear portion of the stress-strain curve. Sample geometries were as follows: gauge length =

14.75 mm, width = 3.00 mm, thickness = 0.40 mm. Reported moduli are the average of three different samples of each polymer

4.9 FABRICATION OF 3-POINT BENDING SAMPLES

A strip of aluminum 1 cm wide by 7.5 cm long was cut from sheet stock and the edges were filed to remove any burrs that could interfere with coating. The strip was then polished with hexanes and acetone and clamped to a smooth high density polyethylene plate. A thick bead of ionomer solution was applied across the width of the strip and a pulldown bar was drawn down the length of the strip in one smooth motion. Pulldown bars with spacings of 0.17 mm, 0.34 mm, and 0.75 mm were utilized to fabricate samples of consistent thickness by subsequently drawing down polymer solution with increasing pulldown bar spacing until the total thickness of the sample reached approximately 0.60 mm. Between each application of the polymer solution, the entire plate was transferred to a 60 °C oven until the solution became slightly tacky. Following the final application of solution, the plate was transferred to the oven until the sample was dry to the touch. The sample was then physically removed with a razor blade and excess polymer was trimmed. Typical final sample dimensions were 80 x 19 x 1.2 mm.

4.10 FLEXURAL MODULUS MEASUREMENTS

Prior to data collection, each sample was dried in a vacuum oven and conditioned in a sealed vessel containing a saturated LiCl solution (11% relative humidity) for three days to ensure a

consistent water content.[54] Flexural modulus measurements of both unbiased and biased samples were carried out on a custom-built three-point bending apparatus controlled by MathWorks's MATLAB software. A stepper motor displaced the sample at a constant rate and a 10 lb load cell measured the force required to bend the sample. Measurements were obtained in a dry nitrogen atmosphere to prevent the atmospheric wetting of the surface of the sample. Force vs. displacement data was plotted and the slope of the resulting line was used to calculate the effective flexural modulus of the sample as per Timoshenko beam theory. Each measurement was taken in triplicate in order to determine reproducibility of the process. Biased samples were tested by sandwiching the samples between glass slides and applying a preload to force intimate contact of the surfaces prior to applying a potential. Glass slides were removed and the flexural modulus of the sample was measured as before. Before applying each subsequent potential, the sandwich structure was separated in order to dissipate any residual adhesion and provide a fresh interface for charging.

APPENDIX A

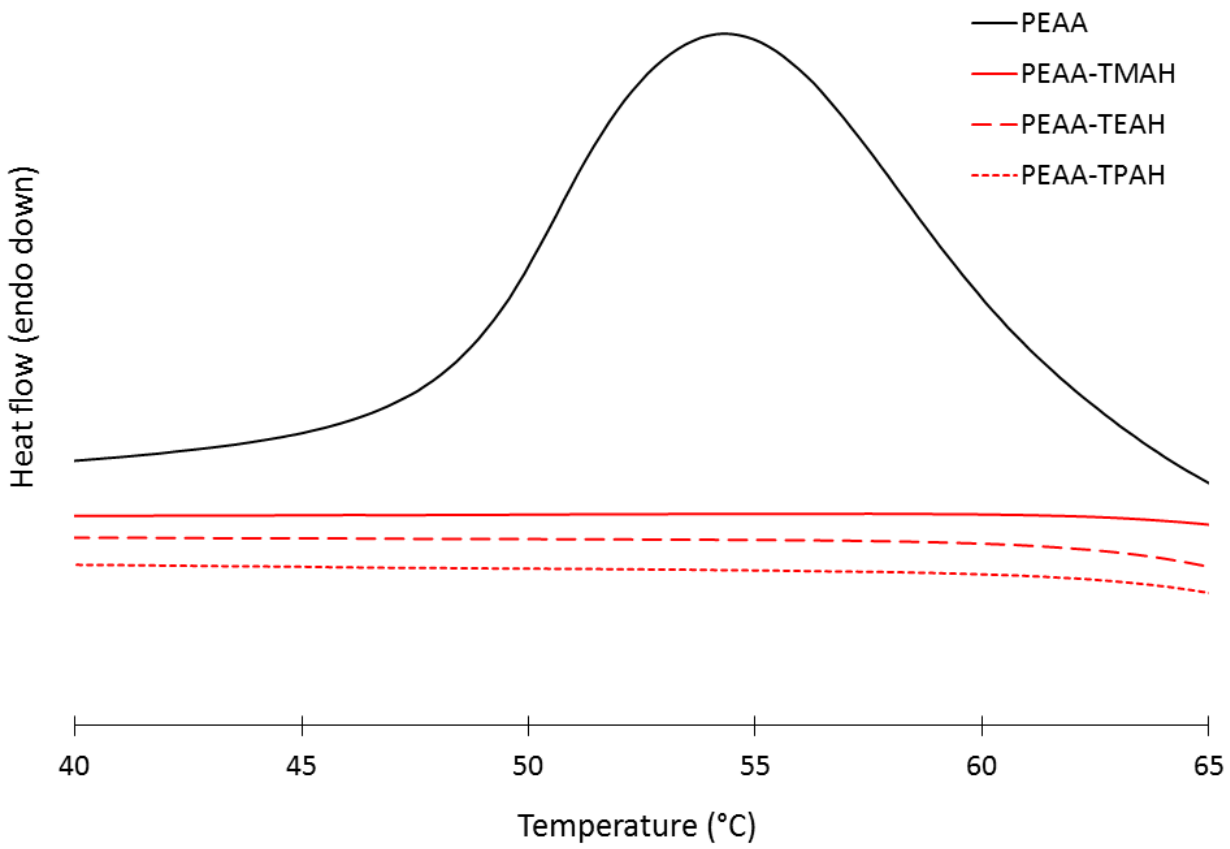

Figure 18. Second cooling cycle of DSC thermogram.

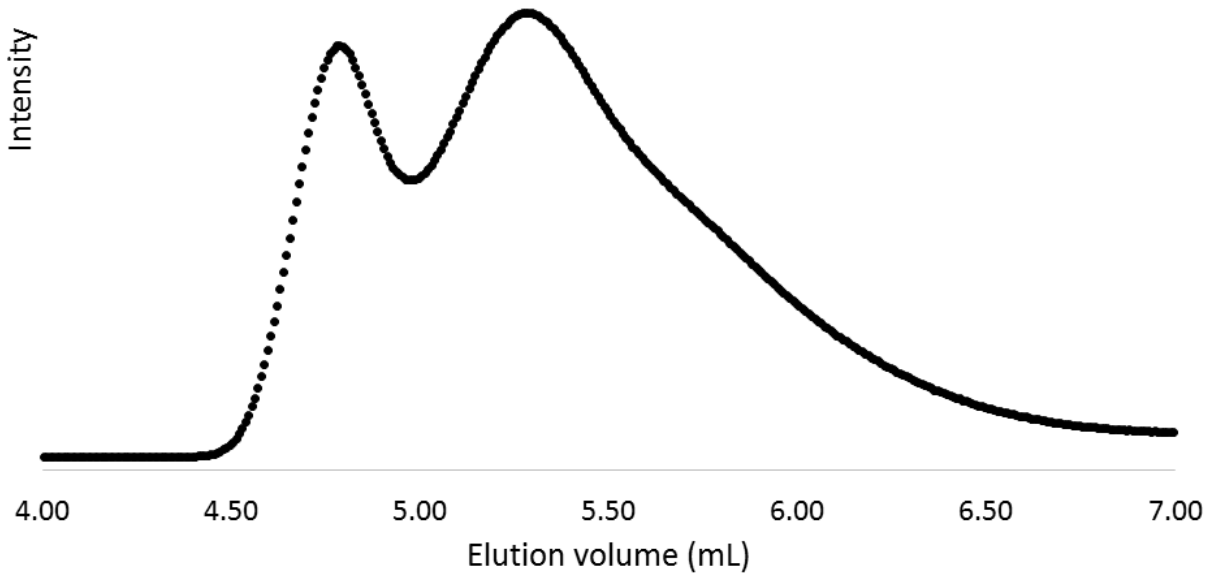

Figure 19. Size-exclusion chromatograph of PEAA in THF.

BIBLIOGRAPHY

1. Stuart, M. A. C.; Huck, W. T. S.; Genzer, J.; Muller, M.; Ober, C.; Stamm, M.; Sukhorukov, G. B.; Szleifer, I.; Tsukruk, V. V.; Urban, M.; Winnik, F.; Zauscher, S.; Luzinov, I.; Minko, S., Emerging applications of stimuli-responsive polymer materials. *Nat Mater* **2010,** *9* (2), 101-113.

2. Jhaveri, S. J.; Hynd, M. R.; Dowell-Mesfin, N.; Turner, J. N.; Shain, W.; Ober, C. K., Release of Nerve Growth Factor from HEMA Hydrogel-Coated Substrates and Its Effect on the Differentiation of Neural Cells. *Biomacromolecules* **2009,** *10* (1), 174-183.

3. Han, L.-H.; Lai, J. H.; Yu, S.; Yang, F., Dynamic tissue engineering scaffolds with stimuli-responsive macroporosity formation. *Biomaterials* **2013,** *34* (17), 4251-4258.

4. Tokarev, I.; Minko, S., Stimuli-responsive hydrogel thin films. *Soft Matter* **2009,** *5* (3), 511-524.

5. Rajagopalan, M.; Jeon, J.-H.; Oh, I.-K., Electric-stimuli-responsive bending actuator based on sulfonated polyetherimide. *Sensors and Actuators B: Chemical* **2010,** *151* (1), 198-204.

6. Bhowmick, A. K.; De, S. K.; Naskar, A. K., Thermoplastic Elastomeric Composition Based on Ground Rubber Tire. *Polymer Engineering and Science* **2001,** *41*, 1087.

7. Lackey, C. A.; Murthy, N.; Press, O. W.; Tirrell, D. A.; Hoffman, A. S.; Stayton, P. S., Hemolytic Activity of pH-Responsive Polymer-Streptavidin Bioconjugates. *Bioconjugate Chemistry* **1999,** *10* (3), 401-405.

8. Murdan, S., Electro-responsive drug delivery from hydrogels. *Journal of Controlled Release* **2003,** *92* (1–2), 1-17.

9. Calvo-Marzal, P.; Delaney, M. P.; Auletta, J. T.; Pan, T.; Perri, N. M.; Weiland, L. M.; Waldeck, D. H.; Clark, W. W.; Meyer, T. Y., Manipulating Mechanical Properties with Electricity: Electroplastic Elastomer Hydrogels. *ACS Macro Letters* **2012,** *1* (1), 204-208.

10. Harris, R. D.; Auletta, J. T.; Motlagh, S. A. M.; Lawless, M. J.; Perri, N. M.; Saxena, S.; Weiland, L. M.; Waldeck, D. H.; Clark, W. W.; Meyer, T. Y., Chemical and Electrochemical Manipulation of Mechanical Properties in Stimuli-Responsive Copper-Cross-Linked Hydrogels. *ACS Macro Letters* **2013,** *2* (12), 1095-1099.

11. Auletta, J. T.; LeDonne, G. J.; Gronborg, K. C.; Ladd, C. D.; Liu, H.; Clark, W. W.; Meyer, T. Y., Stimuli-Responsive Iron-Cross-Linked Hydrogels That Undergo Redox-Driven Switching between Hard and Soft States. *Macromolecules* **2015,** *48* (6), 1736-1747.

12. Bar-Cohen, Y.; Zhang, Q., Electroactive Polymer Actuators and Sensors. *MRS Bulletin* **2008,** *33* (03), 173-181M3 - 10.1557/mrs2008.42.

13. Pipes, R. B.; Pagano, N. J., Interlaminar Stresses in Composite Laminates Under Uniform Axial Extension. *Journal of Composite Materials* **1970,** *4* (4), 538-548.

14. Bergamini, A.; Christen, R.; Maag, B.; Motavalli, M., A sandwich beam with electrostatically tunable bending stiffness. *Smart Materials and Structures* **2006,** *15* (3), 678.

15. Bergamini, A.; Christen, R.; Motavalli, M., Electrostatically tunable bending stiffness in a GFRP–CFRP composite beam. *Smart Materials and Structures* **2007,** *16* (3), 575.

16. Ginés, R.; Bergamini, A.; Christen, R.; Motavalli, M.; Ermanni, P., Frictional behaviour of polymer films under mechanical and electrostatic loads. *Smart Materials and Structures* **2013,** *22* (7), 075023.

17. Sogard, M. R.; Mikkelson, A. R.; Ramaswamy, V.; Engelstad, R. L., Analysis of Coulomb and Johnsen-Rahbek electrostatic chuck performance in the presence of particles for extreme ultraviolet lithography. *MOEMS* **2009,** *8* (4), 041506-041506-9.

18. Armand, M.; Tarascon, J. M., Issues and challenges facing rechargeable lithium batteries. *Nature* **2001,** *414*, 359+.

19. Gao, L.; Seliskar, C. J., Formulation, Characterization, and Sensing Applications of Transparent Poly(vinyl alcohol)−Polyelectrolyte Blends. *Chemistry of Materials* **1998,** *10* (9), 2481-2489.

20. Qin, S.; McTeer, A., Wafer dependence of Johnsen–Rahbek type electrostatic chuck for semiconductor processes. *Journal of Applied Physics* **2007,** *102* (6), 064901.

21. Chu, B.; Zhou, X.; Ren, K.; Neese, B.; Lin, M.; Wang, Q.; Bauer, F.; Zhang, Q. M., A Dielectric Polymer with High Electric Energy Density and Fast Discharge Speed. *Science* **2006,** *313* (5785), 334-336.

22. Watanabe, M.; Sanui, K.; Ogata, N.; Kobayashi, T.; Ohtaki, Z., Ionic conductivity and mobility in network polymers from poly(propylene oxide) containing lithium perchlorate. *Journal of Applied Physics* **1985,** *57* (1), 123.

23. Cohen, M. H.; Turnbull, D., Molecular Transport in Liquids and Glasses. *The Journal of Chemical Physics* **1959,** *31* (5), 1164-1169.

24. Ohno, H.; Yoshizawa, M.; Ogihara, W., Development of new class of ion conductive polymers based on ionic liquids. *Electrochimica Acta* **2004,** *50* (2–3), 255-261.

25. Tudryn, G. J.; Liu, W.; Wang, S.-W.; Colby, R. H., Counterion Dynamics in Polyester−Sulfonate Ionomers with Ionic Liquid Counterions. *Macromolecules* **2011,** *44* (9), 3572-3582.

26. Kremer, F. S., A., *Broadband Dielectric Spectroscopy*. Springer: New York, 2003.

27. Asano, K.; Hatakeyama, F.; Yatsuzuka, K. In *Fundamental study of an electrostatic chuck for silicon wafer handling*, Industry Applications Conference, 1997. Thirty-Second IAS Annual Meeting, IAS '97., Conference Record of the 1997 IEEE, 5-9 Oct 1997; 1997; pp 1998-2003 vol.3.

28. Shim, G. I.; Sugai, H., Dechuck Operation of Coulomb Type and Johnsen-Rahbek Type of Electrostatic Chuck Used in Plasma Processing. *Plasma and Fusion Research* **2008,** *3*, 051-051.

29. George, E. Z. A Novel Method for Measuring Electrostatic Adhesion in Multi-Layer Polymer Structures. University of Pittsburgh, 2014.

30. Eaton, W. P.; Bitsie, F.; Smith, J. H.; Plummer, D. W. In *A New Analytical Solution for Diaphragm Deflection and its Application to a Surface-Micromachined Pressure Sensor*, International Conference on Modeling and Simulation of Microsystems, Albuquerque, NM, Albuquerque, NM, 1999; p 4.

31. Karger-Kocsis, J.; Varga, J.; Ehrenstein, G. W., Comparison of the fracture and failure behavior of injection-molded α- and β-polypropylene in high-speed three-point bending tests. *Journal of Applied Polymer Science* **1997,** *64* (11), 2057-2066.

32. ASTM, Standard Test Methods for Flexural Properties of Unreinforced and Reinforced Plastics and Electrical Insulating Materials. ASTM International: 2010; Vol. Standard D790.

33. Cipriano, R. A.; Longoria, J. J., Electroresponsive polymer systems. Google Patents: 1996.

34. Green, M. D.; Salas-de la Cruz, D.; Ye, Y.; Layman, J. M.; Elabd, Y. A.; Winey, K. I.; Long, T. E., Alkyl-Substituted N-Vinylimidazolium Polymerized Ionic Liquids: Thermal Properties and Ionic Conductivities. *Macromolecular Chemistry and Physics* **2011,** *212* (23), 2522-2528.

35. Ke, Q.-q.; Jiang, P.-k.; Wei, P.; Wang, G.-l.; Kim, C.-n., MODIFICATION OF POLYETHYLENE BY in situ FORMED SODIUM ACRYLATE. *Chinese Journal of Polymer Science (World Scientific Publishing Company)* **2006,** *24* (6), 559-567.

36. Baughman, T. W.; Chan, C. D.; Winey, K. I.; Wagener, K. B., Synthesis and Morphology of Well-Defined Poly(ethylene-co-acrylic acid) Copolymers. *Macromolecules* **2007,** *40* (18), 6564-6571.

37. Rúan-Esparza, L.; Soto, V.; Gómez-Salazar, S.; Rabelero, M.; Ávalos-Borja, M.; Luna-Bárcenas, G.; Prokhorov, E.; Nuño-Donlucas, S. M., Poly[ethylene-co-(acrylic acid)]-based nanocomposites: Thermal and mechanical properties and their structural characteristics studied by Raman spectroscopy. *Polymer Composites* **2011,** *32* (8), 1181-1189.

38. Hirasawa, E.; Yamamoto, Y.; Tadano, K.; Yano, S., Effect of metal cation type on the structure and properties of ethylene ionomers. *Journal of Applied Polymer Science* **1991,** *42* (2), 351-362.

39. Weiss, R. A.; Agarwal, P. K.; Lundberg, R. D., Control of ionic interactions in sulfonated polystyrene ionomers by the use of alkyl-substituted ammonium counterions. *Journal of Applied Polymer Science* **1984,** *29* (9), 2719-2734.

40. Verevkin, S.; Beckhaus, H.-D.; Schüle, U.; Rüchardt, C., Experimental Enthalpies of Formation and Strain of the Methylated 1-Amino-2-phenylethanes. *Structural Chemistry* **1998,** *9* (1), 1-7.

41. Macdonald, J. R.; Barsoukov, E., Impedance spectroscopy: theory, experiment, and applications. *History* **2005,** *1*, 8.

42. Coorstek, Aluminum nitride substrates. Assembly, T. M. M., Ed. 2013.

43. Inc., F.-C. G., Ceramic Properties Tables. Ferro-Ceramic Grinding, I., Ed. 2012.

44. Tecaflon Tecaflon PVDF (Polyvinylidene Fluoride). https://www.plasticsintl.com/datasheets/PVDF.pdf.

45. Bettacchi, P.; Montanari, D.; Zanarini, D.; Orioli, D.; Rondelli, G.; Sanua, A. In *Power Film Capacitors for Industrial Applications*, Proceedings CARTS Europe 2010 - Symposium for Passive Electronics, Munich, GE, Munich, GE, 2010.

46. stericKimpton, J.; Randle, T. H.; Drennan, J., Investigation of electrical conductivity as a function of dopant-ion radius in the systems Zr0.75Ce0.08M0.17O1.92 (M=Nd, Sm, Gd, Dy, Ho, Y, Er, Yb, Sc). *Solid State Ionics* **2002,** *149* (1–2), 89-98.

47. Marcus, Y., Tetraalkylammonium Ions in Aqueous and Non-aqueous Solutions. *J Solution Chem* **2008,** *37* (8), 1071-1098.

48. Stevens, M. P., *Polymer Chemistry: An Introduction*. Addison-Wesley Publishing Company, Advanced Book Program: 1975.

49. Yuan, J.; Antonietti, M., Poly(ionic liquid)s: Polymers expanding classical property profiles. *Polymer* **2011,** *52* (7), 1469-1482.

50. Pinaud, J.; Vignolle, J.; Gnanou, Y.; Taton, D., Poly(N-heterocyclic-carbene)s and their CO2 Adducts as Recyclable Polymer-Supported Organocatalysts for Benzoin Condensation and Transesterification Reactions. *Macromolecules* **2011,** *44* (7), 1900-1908.

51. Carlisle, T. K.; McDanel, W. M.; Cowan, M. G.; Noble, R. D.; Gin, D. L., Vinyl-Functionalized Poly(imidazolium)s: A Curable Polymer Platform for Cross-Linked Ionic Liquid Gel Synthesis. *Chemistry of Materials* **2014,** *26* (3), 1294-1296.

52. Ngo, H. L.; LeCompte, K.; Hargens, L.; McEwen, A. B., Thermal properties of imidazolium ionic liquids. *Thermochimica Acta* **2000,** *357–358* (0), 97-102.

53. Ohno, H., Design of Ion Conductive Polymers Based on Ionic Liquids. *Macromolecular Symposia* **2007,** *249-250* (1), 551-556.

54. Greenspan, L., Humidity Fixed Points of Binary Saturated Aqueous Solutions. *Journal of Research of the National Bureau of Standards - A. Physics and Chemistry* **1976,** *81A* (1), 8.